



Diurnal variability of the global tropical tropopause: results inferred from COSMIC observations

K. V. Suneeth¹ · Siddarth Shankar Das¹ · Subrata Kumar Das²

Received: 22 March 2016 / Accepted: 21 December 2016 / Published online: 21 January 2017
© Springer-Verlag Berlin Heidelberg 2017

Abstract Short and long-term variability of the tropical tropopause controls the exchange of minor constituents between the troposphere and the stratosphere. We present the diurnal variability of the global tropical tropopause altitude and temperature using 7 years of COSMIC observations. The aim of the study is to extract diurnal tropopause signals and their impact on stratosphere-troposphere exchange processes. The possible role of atmospheric tides and convection in controlling the tropopause characteristics are discussed. The most significant and new observation is that in the deep tropics the cold-point tropopause altitude is higher and temperature is cooler over the land (ocean) during evening to late evening hours (afternoon to early evening). Lower tropopause altitude allows the stratospheric air intrusion into the troposphere during the day time. The combined effect of diurnal tropopause altitude changes and turbulent mixing increases the possibility of stratospheric intrusions. A warmer forenoon tropopause allows increased injection of water vapor from the troposphere to the lower stratosphere. Over the tropical land (ocean), the zonal mean diurnal amplitude is 130–200 m (140–180 m) for tropopause altitude and 0.6–0.9 K (0.6–0.8 K) for tropopause temperature.

Keywords Tropopause · Stratosphere–troposphere exchange · Diurnal variability · COSMIC

✉ Siddarth Shankar Das
dassiddhu@yahoo.com

¹ Space Physics Laboratory, Vikram Sarabhai Space Centre, ISRO PO, Trivandrum 695022, India

² PM & A Division, Indian Institute of Tropical Meteorology, Pune 411008, India

1 Introduction

In the recent decades, there has been a renewing interest to understand the dynamical characteristics of the tropopause, especially in the tropical region. The tropopause is a natural temperature inversion layer which separates the well-mixed troposphere from the stably stratified stratosphere. There are several definitions for the tropopause on the basis of its chemical, dynamical and thermal structure. Among these definitions, the cold-point tropopause (CPT) and the lapse-rate tropopause (LRT) introduced by the World Meteorological Organization (WMO) are widely used. The Brewer-Dobson circulation (BDC) is one of the responsible mechanisms for the transport of air masses from the troposphere to the lower stratosphere in the tropics. During this transport, the tropical tropopause temperature plays an important role in controlling the injection of water vapor into the lower stratosphere (Jain et al. 2006; Fueglistaler et al. 2009; Uma et al. 2013a, 2014). The minor changes in the stratospheric water vapor may have a significant effect on the stratospheric chemistry and the global radiation budget (Holton et al. 1995; Forster and Shine 1999). Recent studies using the tropical tropopause characteristics have shown a widening of the tropical belt associated with climate change (Seidel et al. 2008; Seidel and Randel 2006; Birner 2010). Increased area of upwelling, caused by the widening of tropical belt, together with flux strength, can lead to enhanced water vapor transport into the stratosphere. More stratospheric water vapor reduces the stratospheric ozone (Kirk-Davidoff et al. 1999). Rind and Lonergan (1995) established that a doubling in stratospheric water vapor cools the stratosphere by 2–3 K and warms the upper troposphere by 0.5 K. Therefore, monitoring of the global tropical tropopause structure, altitude, and its variability can provide a better understanding on the

stratosphere–troposphere exchange (STE) processes and throw light on climate change.

Owing to the importance of the tropopause characteristics and its variability in space and time, it has been studied with a variety of data sets, viz. radiosonde, radar observations, radio occultation, and models. There are many studies which deal with the variation of the tropopause on time scales of annual (e.g. Seidel et al. 2001 and references therein), seasonal (e.g. Liu et al. 2014), monthly (e.g. Rieckh et al. 2014 and reference therein) and day-to-day (e.g. Jain et al. 2006). Seidel and Randel (2006) noticed that the tropopause altitude is negatively correlated with the stratospheric temperature variations and positively correlated with the tropospheric temperature variations on monthly and synoptic timescales. The tropical tropopause also responds to the equatorial waves, viz. Kelvin waves (Tsuda et al. 1994) and Rossby-gravity waves (Fujiwara et al. 2012). In addition, the tropopause structure is modulated by the breaking of Rossby waves on the isentropic surface (Scott and Cammas 2002). Shimizu and Tsuda (2000) have demonstrated the effect of Madden-Julian oscillation (MJO) on the tropopause altitude. The annual variability of the tropopause is affected by the solar radiation received at the Earth's surface. Earlier studies have shown that the interannual variations in the tropopause are associated with the Quasi-Biennial Oscillation (QBO) (Das et al. 2012; Rieckh et al. 2014) and the El-Nino Southern oscillation (ENSO) (Gage and Reid 1985). The effect of convection on the tropopause characteristics is discussed by Gettelman et al. (2002).

Stratosphere-Troposphere Exchange (STE), which is the two-way transport of air mass and chemical species (Holton et al. 1995) is mainly controlled by the tropopause parameters like altitude, temperature, and pressure. Investigation of diurnal variability in various atmospheric parameters is very important to understand the dynamical and chemical processes in the Earth's atmosphere (e.g. Xie et al. 2010). Hence, the studies on the diurnal variability are necessary for better quantification of STE. However, there are very limited studies so far reported on the diurnal variability of the tropical tropopause (e.g. Yamamoto et al. 2003; Das et al. 2008). Globally, the radiosonde observations are made twice in a day, viz. at 00 GMT and 12 GMT, which is not sufficient enough to study the diurnal variability of tropopause. To overcome these difficulties, Very-High Frequency (VHF) radars are used to study the tropical tropopause. Yamamoto et al. (2003) and Das et al. (2008, 2010) have successfully demonstrated the capability of the VHF radar to study the variability of the tropical tropopause in smaller time scale (~3-h). Globally, a very few VHF radars exist and thus, this conventional technique cannot be used to study the global characteristics of the tropopause on a diurnal scale.

The space-borne Global Positioning System-Radio Occultation (GPS-RO) technique is a powerful tool for inferring the vertical structure of the atmospheric temperature and humidity under all weather conditions (Kursinski et al. 1997). In the present study, temperature profile obtained (moist air retrieval) from Constellation Observing System for Meteorology, Ionosphere, and Climate (COSMIC) is used to derive the tropopause altitude and temperature from December-2006 to November-2013. 1 month of COSMIC observations is required to get the composite profile of one diurnal cycle (Xie et al. 2010). This study is the first of its kind to show the diurnal variability of the global tropical tropopause. The paper is organized as: brief descriptions of the COSMIC satellite and data analysis are provided in Sect. 2, methodology and detection of the tropopause are discussed in Sect. 3, followed by observational results and discussion in Sects. 4 and 5, respectively. Section 6 deals with the summary and concluding remarks.

2 Data analysis

2.1 GPS-RO COSMIC

The COSMIC is a joint project by National Aeronautics and Space Administration (NASA) and National Space Organization (NSPO) of Taiwan. Six low-Earth Orbiting (LEO) satellites were launched in 2006, which can track GPS signals to provide information about atmospheric variables. The COSMIC mission is based on the limb viewing radio occultation technique. The LEO satellites continuously receive and track GPS radio signals during an occultation event. In addition to relative motion of the satellites, the refraction due to the neutral atmosphere and the ionosphere induces a Doppler shift, in the received signal at the LEO satellite. After applying the ionosphere correction, changes in phase due to the neutral atmosphere is then extracted which is further used to estimate the bending angle as a function of tangential height. Further, bending angle is converted into refractivity (N) by using Abel transform. At microwave frequencies, refractivity of the neutral atmosphere can be approximated using Eq. (1) (Smith and Weintraub 1953).

$$N = b_1 \frac{P}{T} + b_2 \frac{P_w}{T^2} \quad (1)$$

where $b_1 = 77.6 \text{ K hPa}^{-1}$, $b_2 = 3.73 \times 10^5 \text{ K}^2 \text{ hPa}^{-1}$, P is the pressure in hPa, T is the temperature in K and P_w is the water vapor partial pressure in hPa. From the refractivity profiles, temperature profiles can be obtained by using Eq. (1). The temperature profile obtained by neglecting the second term in Eq. (1) is named as dry-air retrieval, whereas the one obtained by considering the second term

is named as moist-air retrieval (also known as **wetPrf**). A one-dimensional variational retrieval method (1DVar) is used to obtain the **wetPrf** with background information, at the COSMIC Data Analysis and Archive Center (CDAAC). Detailed methodology of GPS-RO technique, temperature, and pressure estimation can be found elsewhere (Kursinski et al. 1997).

The vertical resolution in the GPS-RO measurement varies with the retrieval techniques. The GPS-RO technique has two retrieval algorithms i.e. (1) Geometrical Optics (GO) method and (2) Radio Holographic (RH) method. In GO method, the vertical resolution is limited by Fresnel radius; it is found to be ~0.5 km in the lower troposphere and ~1.4 km in the upper troposphere and the lower stratosphere (UTLS) region (Kursinski et al. 1997). In RH, raw complex signals (phase and amplitude) of RO sounding are used (Kuo et al. 2004) to improve the vertical resolution up to 100–200 m (Tsuda et al. 2011). Both refractivity and temperature measurements in the COSMIC observations have a precision of 0.1% between 8 and 25 km (Alexander et al. 2014). The temperature accuracy in the UTLS is better than 0.5 K for individual profiles and ~0.1 K for averaged profiles (Hajj et al. 2004). Extensive validation of temperature derived from the COSMIC satellite with other in situ observations, reanalysis, and model have been carried out in the past (Kishore et al. 2009; Alexander et al. 2014). Kuo et al. (2004) have provided the detailed description of inversion process used for the COSMIC mission.

In the present study, level 2 temperature profiles from **wetPrf** are used for the period December-2006 to November-2013. The altitude resolution of the COSMIC temperature profile is 100 m. The data are obtained from the COSMIC Data Analysis and Archive Center (CDAAC) (<http://cdaac-www.cosmic.ucar.edu/cdaac/index.html>). Globally, COSMIC provides about 1500–2000 occultations per day; however, in the tropical region (30°N–30°S), about 500 occultations per day are observed.

2.2 IR brightness temperature

The Infrared brightness temperature (IRBT) data (from the Climate Prediction Center/NCEP/NWS) that we have used for the present study is equivalent to black-body temperature. We use the globally-merged IRBT, which is obtained by combining the data from all the available geostationary satellites (GOES-8/10, METEOSAT-7/5, and GMS). The IRBT data which has been corrected for the zenith angle dependencies are available with a very high spatial resolution (4 km×4 km) at every half-hour interval. However, for the present analysis, high-resolution data is reduced to a low-resolution of 2.5°×2.5° with 3-h interval. Details about the data can be found elsewhere (Janowiak et al. 2001 and references therein).

2.3 Aura-MLS

We use the Microwave Limb Sounder (MLS) onboard the Aura satellite for water vapor and ozone profiling. Aura-MLS observes thermal microwave and far-infrared emission from the Earth's atmosphere in 5 spectral regions. Water vapor profile is retrieved from radiance measurements of 190 GHz rotational line. We used version 4.2 level-2 data in which the vertical resolution of water vapor in the range of 1.3 to 3.6 km from 316 to 0.22 hPa. The horizontal resolution along the track varies from 170 to 350 km for the pressure level greater than 4.6 hPa and cross-track is 7 km for all pressure levels. A precision of 15–20%, an accuracy of 8–15% and the minimum of 0.1 ppmv in water vapor measurement is found in version 4.2. Ozone profile is retrieved from radiance measurements near 240 GHz. The vertical resolution is 2.5 km and the horizontal resolution along the track varies from 300 to 450 km and cross track is 6 km. Ozone measurements have a precision of 15–25% and an accuracy of 5%. The equatorial crossing local time of Aura-MLS is about 01:30 AM and 01:30 PM and can provide about 3500 altitude profiles per day. The monthly mean data for day and night are separately analyzed for a grid resolution of 5°×5° from 2007 to 2013. A detailed description of the measurements techniques, resolution, precision, and accuracy can be found in Livesey et al. (2011).

3 Methodology and detection of the tropopause

In the present study, 7 years of temperature data from **wetPrf** are used to examine the global diurnal characteristics of the tropical tropopause. There are six COSMIC satellites and a complete diurnal cycle can be obtained in 10 days at low and mid-latitudes and 1 month for higher latitude (Pirscher et al. 2007; Xie et al. 2010). CPT is defined as the altitude where the tropospheric temperature is minimum (Highwood and Hoskins 1998). LRT is the lowest level at which the average lapse rate between the lowest level to all higher levels within 2 km does not exceed 2 K/km (WMO 1957). The CPT temperature is obtained by taking minimum value of tropospheric temperature in the COSMIC temperature profile of 100 m altitude resolution. Figure 1 shows zonally averaged altitude profile of temperature (color line) and lapse rate (black line) at three different latitudinal belts, i.e. (a) 5°–10°N (tropics) (b) 50°–55°N (mid-latitude), and (c) 75°–80°N (high latitude) on July 4, 2014. The intensity of color line (color code) indicates the temperature lapse rate which is an average of 2 km above it. Horizontal red and black lines indicate the CPT and LRT altitudes respectively. As expected, the tropical CPT and LRT altitude (temperature) are higher (colder) than middle

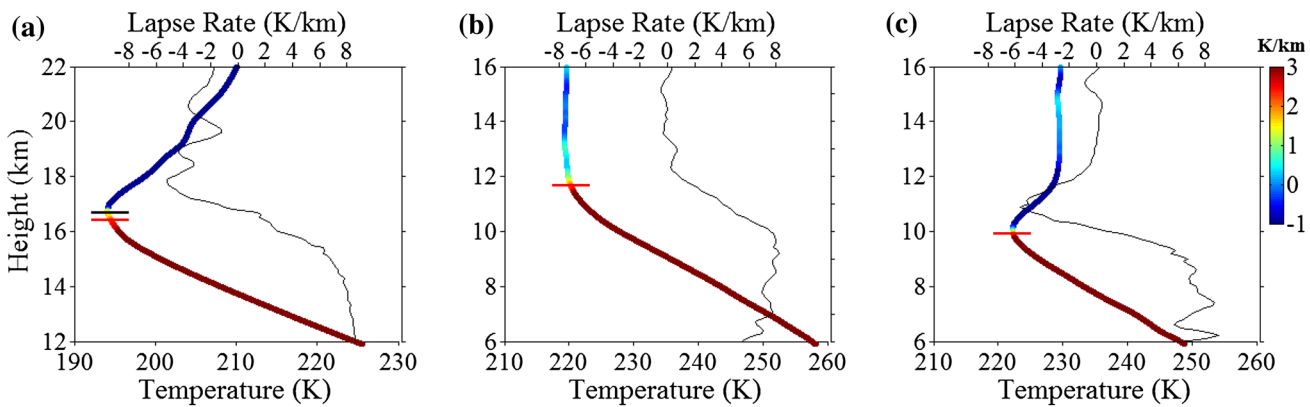


Fig. 1 Zonally averaged altitude profiles of the temperature (thick color line), and lapse rate (thin line) at three different latitudinal belts, i.e. **a** 5° – 10° N **b** 50° – 55° N, and **c** 75° – 80° N on July 4, 2014. The

intensity of colour line indicates the average lapse rate for 2 km. Horizontal line in black indicates the cold-point tropopause (CPT), and red indicates the lapse-rate tropopause (LRT)

and higher latitudes. In the present study, only tropical CPT is considered.

The diurnal cycle is constructed by using equivalent day analysis. For each longitude, time in UTC is converted to local time (LT). The CPT altitude and temperature are grouped into eight local time bins (viz. 0–3, 3–6, 6–9, 9–12, 12–15, 15–18, 18–21 and 21–24 LT). Further, the CPT altitude and temperature are averaged for 2.5° latitude \times 5° longitude grid in each local time bin. The diurnal cycle for each month is a composite of 7 years of data (2007–2013). Grid size is chosen in such a way that there are sufficient numbers of data point in each grid box for diurnal analysis. Total number of data for each grid box in 3 h bin per month for a period of 7 years is about 8–10. In each month, there will be ~ 580 data points per 2.5° latitude band per 3 h bin. Thus, for each month, one total diurnal cycle contains ~ 4640 data points per latitude band in 7 years. Further, the diurnal mean (monthly basis) is removed from every 3 hourly data for individual month (composite of 7 years) to obtain the diurnal variability. The effect of long period oscillation such as quasi-biennial oscillation (QBO) and annual oscillation (AO) are negligible as the data are averaged over 7 years.

4 Observational results

4.1 Geospatial and seasonal characteristics of the CPT

Figure 2 shows the (a) CPT altitude (hereafter CPT-A) and (b) temperature (hereafter CPT-T) at two different timings [day (12–15 LT) and night (0–3 LT)] for January and July in order to investigate the general characteristics of the tropical tropopause. In general, the CPT-A is observed to be higher during January than that of July. For example, the

eastern and western oceanic sides of Amazon show higher CPT-A during January. In contrast to it, during July (Indian summer monsoon month), the CPT-A over the Tibetan plateau (TP) and entire northern India is found to be higher (>18 km) compared to January. Higher tropopause over the TP region is attributed to the presence of anti-cyclone during the Indian summer monsoon (Feng et al. 2011). During night time, the tropopause altitude is found to be higher over the eastern and western oceanic regions of Amazon, whereas over the TP it is high during the day time.

Cold CPT-T is observed in January over the deep tropics during both day and night. Ascending branches of Walker circulation are clearly observed with colder CPT-T as four nodal structures over the Amazon, Central Africa, Maritime Continent and West Pacific. The CPT-T is colder during January and warmer during July which is well reported earlier. It is observed that the CPT-T is colder during the night as compared to the day over the Central Africa during January, which will be discussed in the forthcoming section. The Indian subcontinent and the western Pacific show a distinct diurnal variability during July. These two regions show the coldest CPT-T, whereas rests of the tropics are observed to be relatively warmer in July. Similar features are discussed during the Indian summer monsoon (June–August) over the Bay of Bengal using radiosonde temperature measurement (Jain et al. 2006).

4.2 Latitudinal variation of the CPT

Figure 3 shows the monthly mean diurnal variability of the CPT-A (left) and CPT-T (right) as a function of time, averaged for different latitudinal belts (i.e. 20° – 25° N, 15° – 20° N, 10° – 15° N, 5° – 10° N, 5° S– 5° N, 5° – 10° S, 10° – 15° S, 15° – 20° S, 20° – 25° S.). The deep tropics (5° S– 5° N) and 5° – 10° N show a higher CPT-A in the

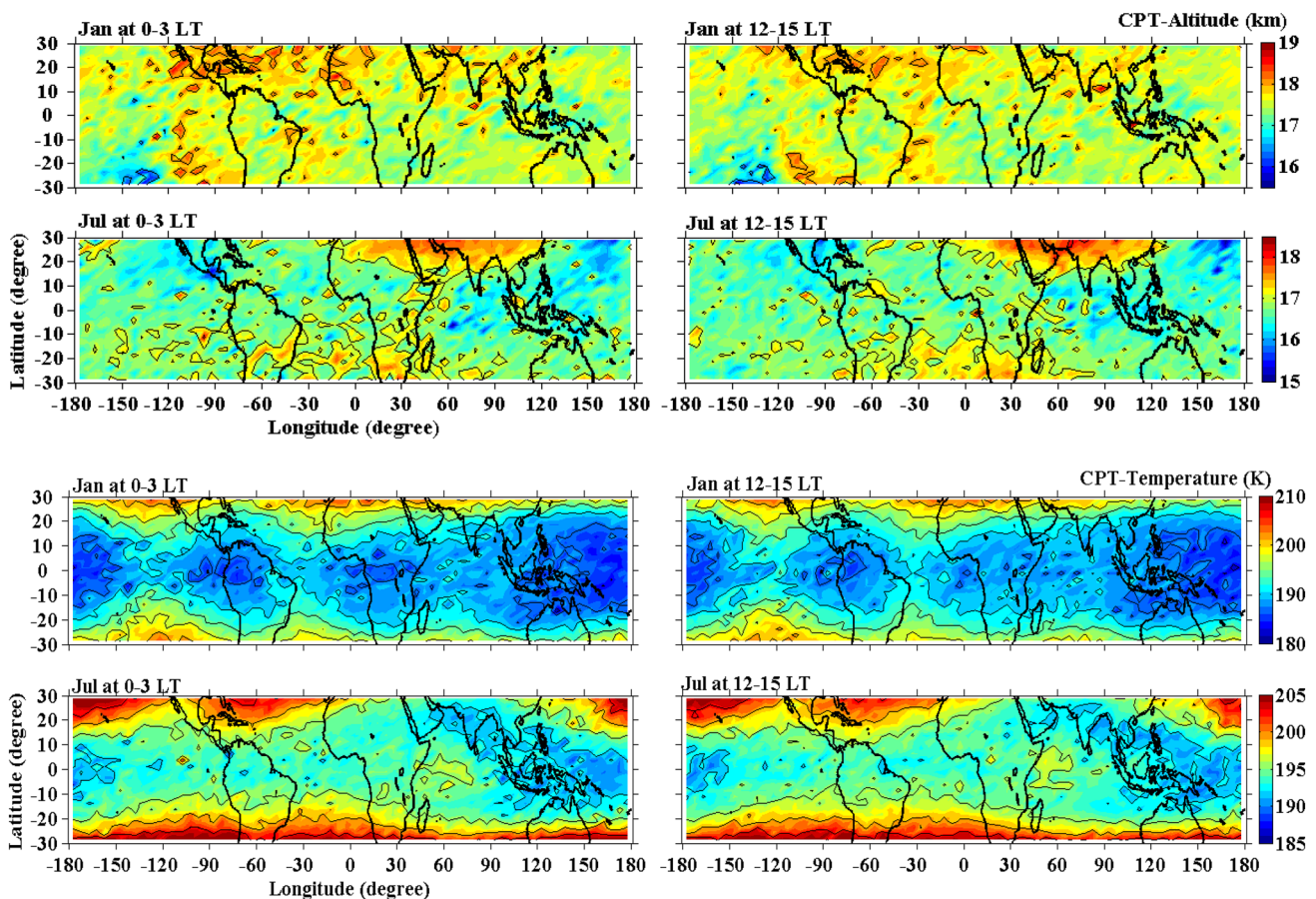


Fig. 2 Latitude-longitude distribution of the cold-point tropopause (CPT) (a) altitude and (b) temperature for January (*top panels*) and July (*bottom panels*) at 0–3 (*left panels*), and 12–15 LT (*right panels*)

evening and late evening hours and a lower CPT-A in the morning and early morning hours, almost in all the seasons. As the latitude increases toward the north, i.e. for 10° – 15° N and 15° – 20° N, a consistent higher CPT-A is not observed in all seasons but limited only to some months. At 20° – 25° N, a weaker diurnal variation is observed except for May and November months. The CPT-A in the Southern Hemisphere (SH) is observed higher between 18 and 24 LT during November to March unlike the Northern Hemisphere (NH), where consistently higher CPT-A is observed throughout the year in the same period. A majority of latitude bands in SH show a higher and lower CPT-A amplitude between 18 and 21 LT and 6–9 LT respectively during January to April.

On the other hand, in the deep tropics and between 5° – 10° N, the warmer CPT-T is observed between 6 and 12 LT. This feature is also observed at 10° – 15° N but the amplitude is less compared to the other two latitude regions (5° S– 5° N and 5° N– 10° N). A diurnal maximum in the CPT-T is observed between 18 and 21 LT as we move towards higher latitudes in the tropical region between

averaged over 2007–2013. The tropopause altitude and temperature shown here is the composite of 7 years (see text for details)

January and April. The SH shows almost similar diurnal variability as in the case for CPT-A but opposite in phase. Diurnal amplitudes of CPT-T are stronger only during austral summer.

4.3 Longitudinal variation of the CPT

Further, the longitudinal distribution of the diurnal variability of the CPT-A and CPT-T for both the NH and SH are separately analyzed. Figure 4 shows the longitudinal distribution of the diurnal variability of CPT-A for the NH (top panels) and SH (bottom panels). Here 0° – 10° N and 0° – 10° S are considered for the NH and SH analysis, respectively. Two distinguished seasons, i.e. December–January–February (DJF) and June–July–August (JJA) are separately analyzed. During the boreal summer (i.e. JJA) in the NH and austral summer (i.e. DJF) in the SH, a higher CPT-A is observed during 15–24 LT. Interestingly, during 3–12 LT, a low CPT-A is clearly observed in the SH during austral summer which is not notable in the NH.

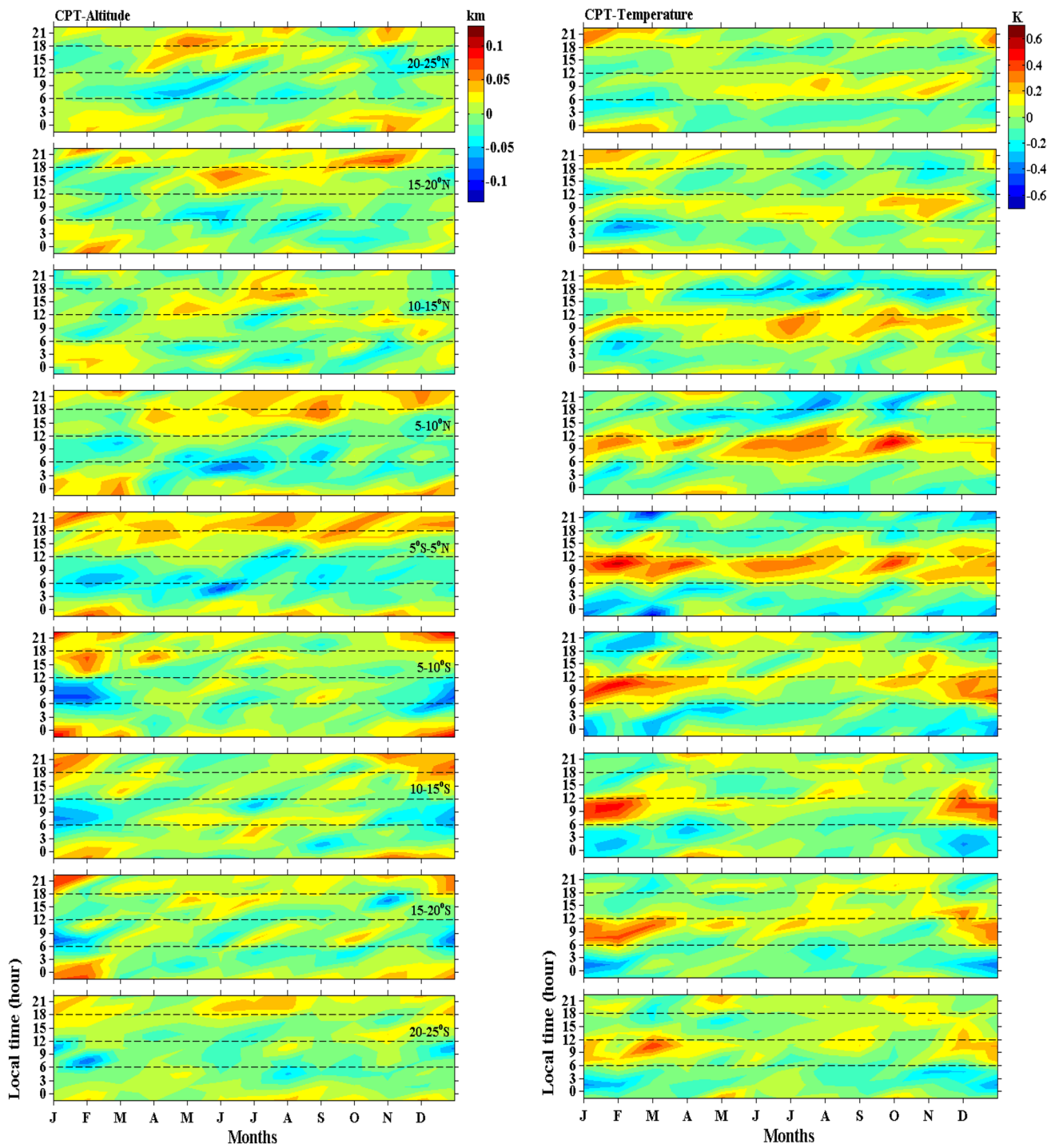


Fig. 3 Zonally averaged diurnal variation of the CPT altitude (*left panels*), and temperature (*right panels*) for different latitude bands for the period from December 2006 to November 2013. *Dashed horizontal lines* on *y* axis indicate 6, 12, and 18 LT

Similarly, Fig. 5 shows the longitudinal variation of the diurnal variability of the CPT-T for both the NH and SH. During the summer season in both the hemispheres, the maximum CPT-T (warm tropopause) is observed during 6–18 LT. Similarly, during boreal winter in the NH and austral winter in the SH, a warmer CPT-T with less variability

is also observed during 6–12 LT but for the region of longitude between -180° and -30° . The coolest tropopause is observed in the SH during austral summer. The average difference between the cool and warm CPT-T in the SH during the austral summer is ~ 1.2 K. The locations of these highest observed variabilities are deep convective regions

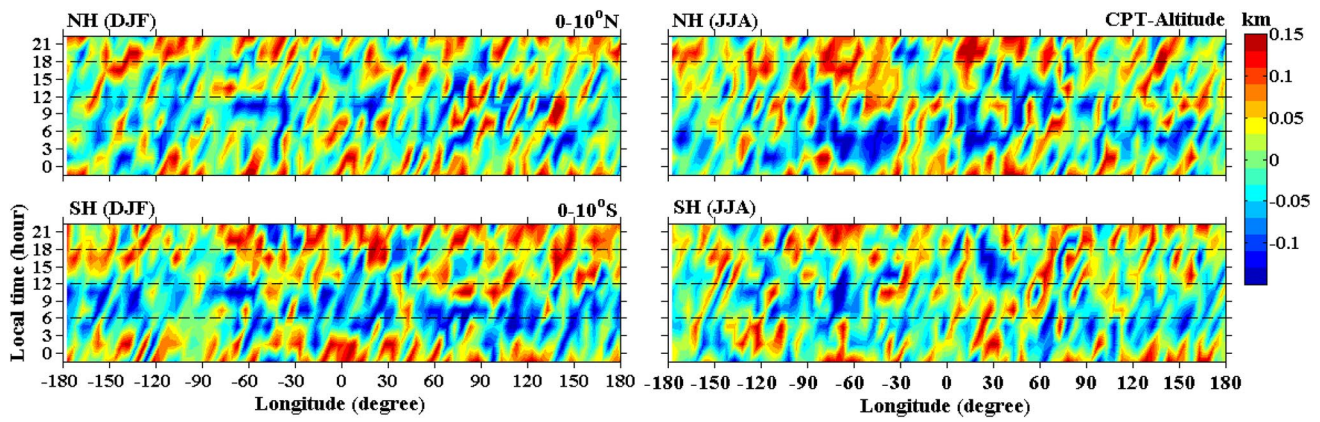


Fig. 4 Longitudinal distribution of diurnal variation of the CPT altitude for Northern Hemisphere (NH) from 0 to 10°N (*top panels*), and Southern Hemisphere (SH) from 0 to 10°S (*bottom panels*)

averaged for two different seasons. The data is composite of 7 years from December 2006 to November 2013. *Dashed horizontal lines* on y-axis indicate 6, 12, and 18 LT

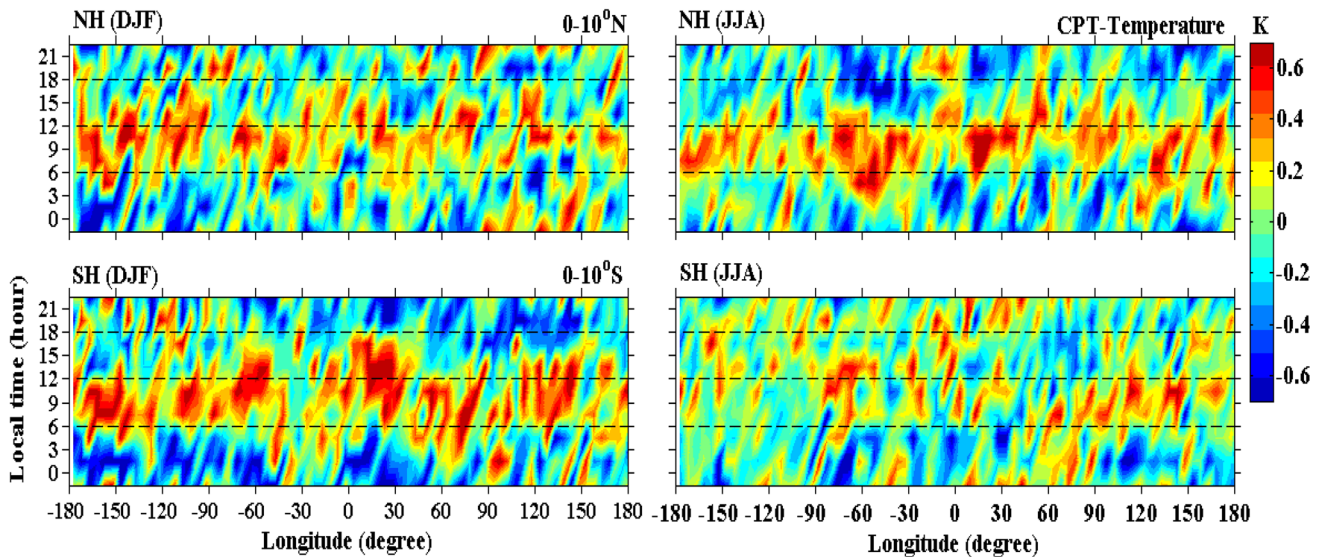


Fig. 5 Same as Fig. 4 but for the CPT temperature

of South American and African continents. Distinct differences in the diurnal variability of the CPT-T are observed compared to CPT-A.

5 Discussion

5.1 Role of tides in the tropopause variability

It is well known that the diurnal variations in the atmospheric parameter are associated with the solar atmospheric tides with a period that is harmonic of one solar day (Chapman and Lindzen 1970). Tides are generated in the tropical troposphere and propagate as internal gravity waves, which

transport energy and momentum from the source. Migrating and non-migrating are the two modes of tidal oscillation in the atmosphere. The migrating tides are Sun-synchronous, which propagate westward. This type of tides are excited by the zonally symmetric absorption of solar radiation by water vapor in the troposphere and ozone in the stratosphere by setting up the thermal forcing (Uma et al. 2013b and reference therein). The non-migrating tides are non-synchronous and are generated due to the zonally asymmetric thermal forcing such as planetary boundary layer heat flux, latent heat release in the tropical troposphere and non-linear interaction between the tides and other propagating waves (Khaykin et al. 2013 and references therein). This mode of tidal oscillation can either propagate eastward or

westward or can stay stationary. Several studies have shown that migrating tides are upper atmosphere phenomena (e.g. Zhang et al. 2006), whereas the non-migrating tides are observed in the UTLS region. Yamamoto et al. (2003) and Das et al. (2008) have proposed that diurnal and semi-diurnal tides are possible causes for the observed diurnal variation in the tropical tropopause altitude. In the present observation, the diurnal variation in the CPT-A and CPT-T could be contributed by non-migrating tides. In addition to the non-migrating tides, locally organized convection may also modulate the tropical tropopause. However, with the present data set contribution from each component cannot be quantified.

5.2 Role of atmospheric convection in controlling the tropopause

The distinct diurnal variability in the tropopause altitude and temperature are in very close association with convection that occurs over the land and ocean (Tian et al. 2004; Biasutti et al. 2012). In the present study, IRBT is used as a proxy for intensity of convection. To get further insight on the connection between the tropopause and convection, we analyzed IRBT for two contrast seasons. Meenu et al. (2010) has proposed that the deep convection cloud top height penetrates above 14 km when IRBT is less than

210 K. Thus, in the present analysis, cloud corresponding to IRBT less than 210 K is considered as deep convective clouds which penetrate above 14 km. Figure 6 shows the peak occurrence timing of deep convective cloud for January and July 2012. It is revealed from the figure that over the land convective activity peaks during the afternoon hours, whereas over the oceans, it peaks in the early morning hours. A detailed study on this aspect is carried out by Biasutti et al. (2012) and Xian and Fu (2015).

Generally, the tropopause altitude is mainly controlled by atmospheric convections and thus, the maximum tropopause altitude is observed in the convective zone, i.e. over the Amazon and Central Africa. In the present analysis, it is observed that CPT-A variability is maximum over the Amazon (between -90° and -30°) and Central Africa (between 0° and 60°) in the summer hemispheres (Fig. 4). Significant diurnal variability in the CPT-A is not found in the winter hemispheres. Similarly, features are also observed in the CPT-T. To get further insight into the role of convection on the tropopause, we have selected two convective regions for each land and ocean, separately. Figure 7 shows the (a) location of land and ocean selected for diurnal variability of CPT-A, CPT-T and percentage of occurrence of IRBT <210 K for (b) January 2012, and (c) July 2012. Different land and oceanic regions (as marked in Fig. 7a) are considered for

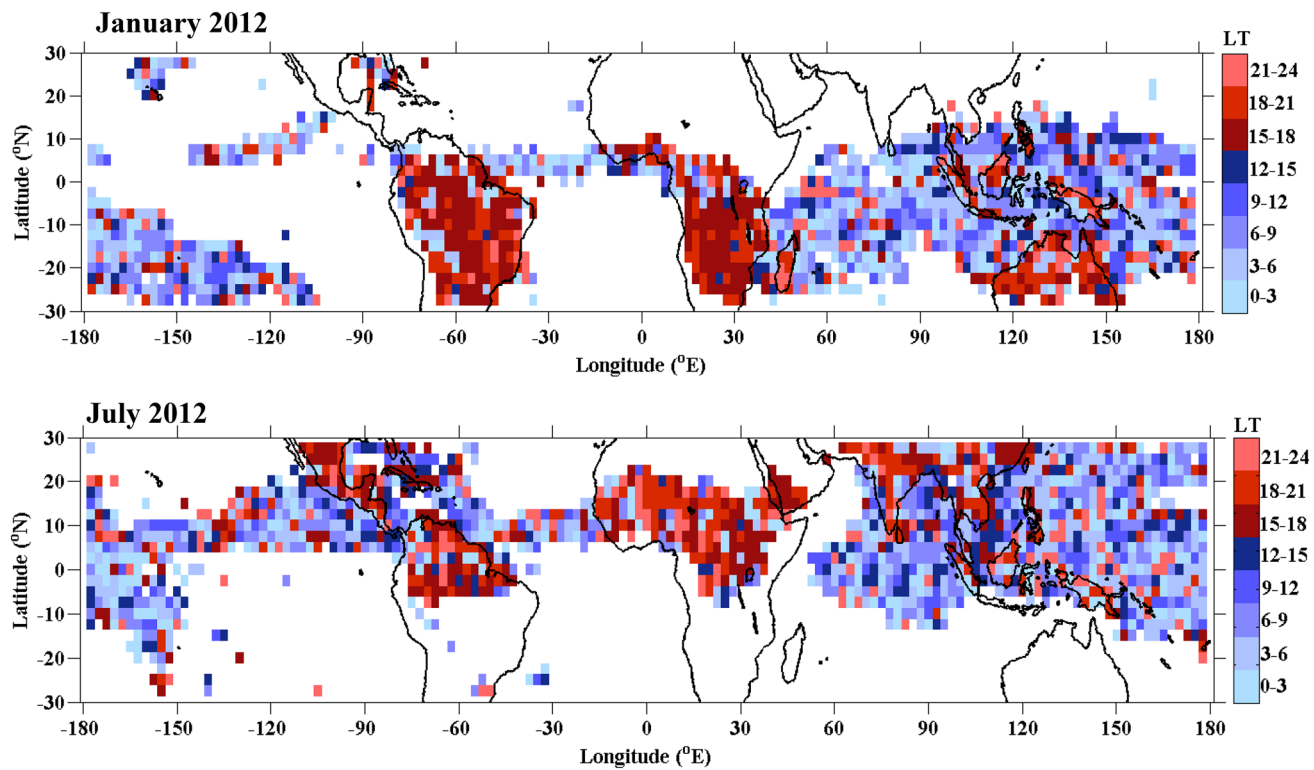


Fig. 6 Peak occurrence timing of deep convective cloud ($\text{Tb} < 210$ K) for January (top) and July (bottom) 2012

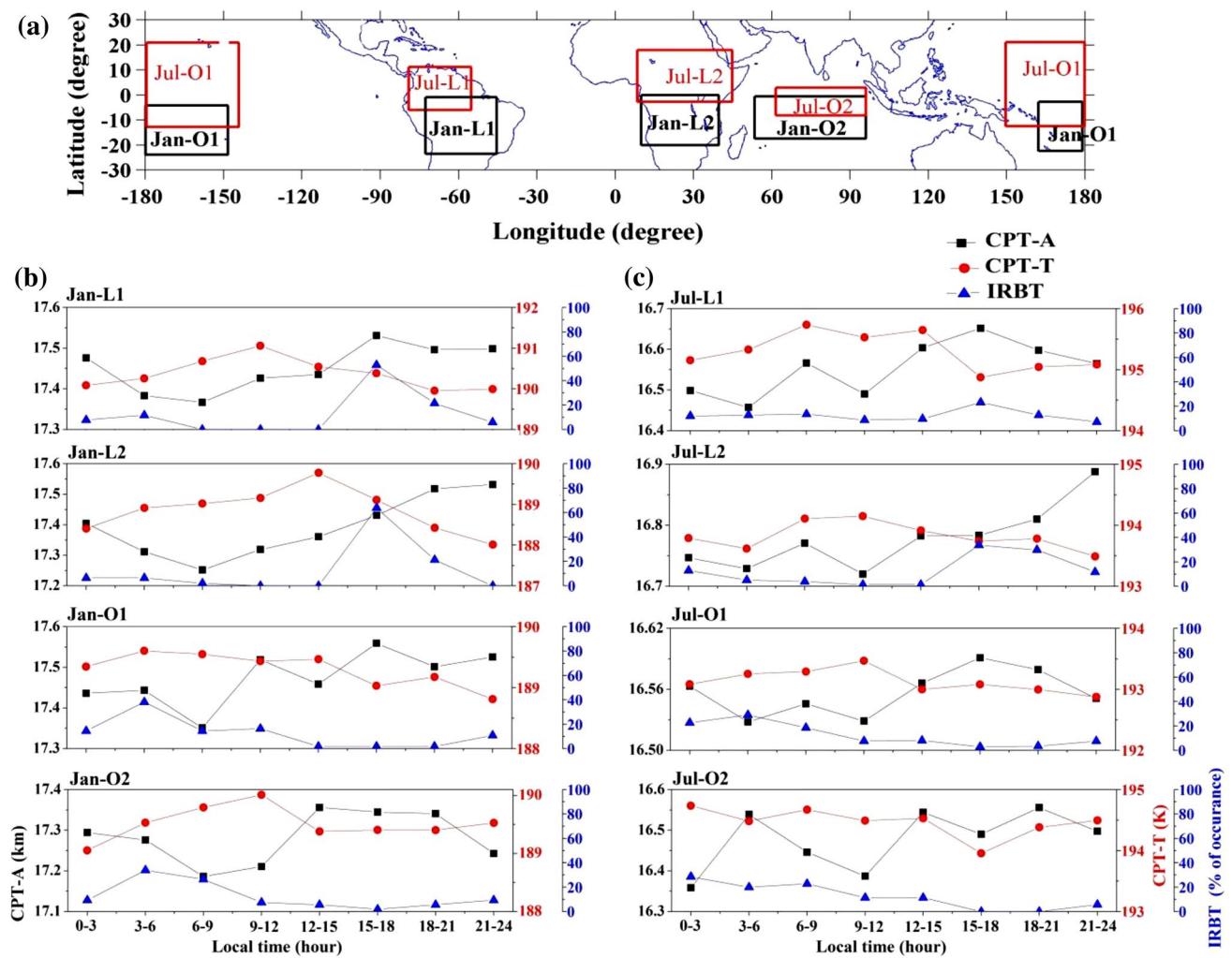


Fig. 7 **a** Location of the land and ocean regions, selected for diurnal variability of CPT-A, CPT-T and percentage of the peak occurrence of IRBT <210 K for **b** January 2012 (black box), and **c** July 2012 (red box)

January and July separately on the basis deep convections (IRBT <210 K). It is revealed from the figure that the tropopause altitude over the land is higher during evening to late evening hours, which is after the peak occurrence time of land convection. Over the ocean, maximum tropopause altitude is observed during afternoon to early evening hours. Diurnal variability over land is found to be higher as compared to the oceans (e.g. Biasutti et al. 2012; Uma and Das 2016). In addition to the convection, the CPT-A may also be influenced by day and night radiative balance (Thuburn and Craig 2002). Over the land, it is observed that the tropopause temperature is warmer~3 h before the peak occurrence time of land convection. Low tropopause temperature observed corresponds to the higher tropopause altitude. The observed low tropopause temperature is attributed to the freeze-dry mechanism, i.e. adiabatic cooling of ascending air

parcel in the vicinity of tropopause during deep convective events.

5.3 Effect of diurnal variability of the tropopause on water vapor and ozone

The tropopause is considered to be a stable layer which acts as an interface between the troposphere (considered to be radiative-convective equilibrium) and the stratosphere (considered to be radiative equilibrium). It controls the two-ways inflow of air-mass and minor constituents between the troposphere and the stratosphere. A major mixing process in the UTLS region takes place in the tropical region, where a large number of convective systems and thunderstorms occur. These convective systems can inject water vapor into the lower stratosphere through the tropical tropopause. It is well known that the stratosphere is highly stable, less turbulent and have subsidence nature

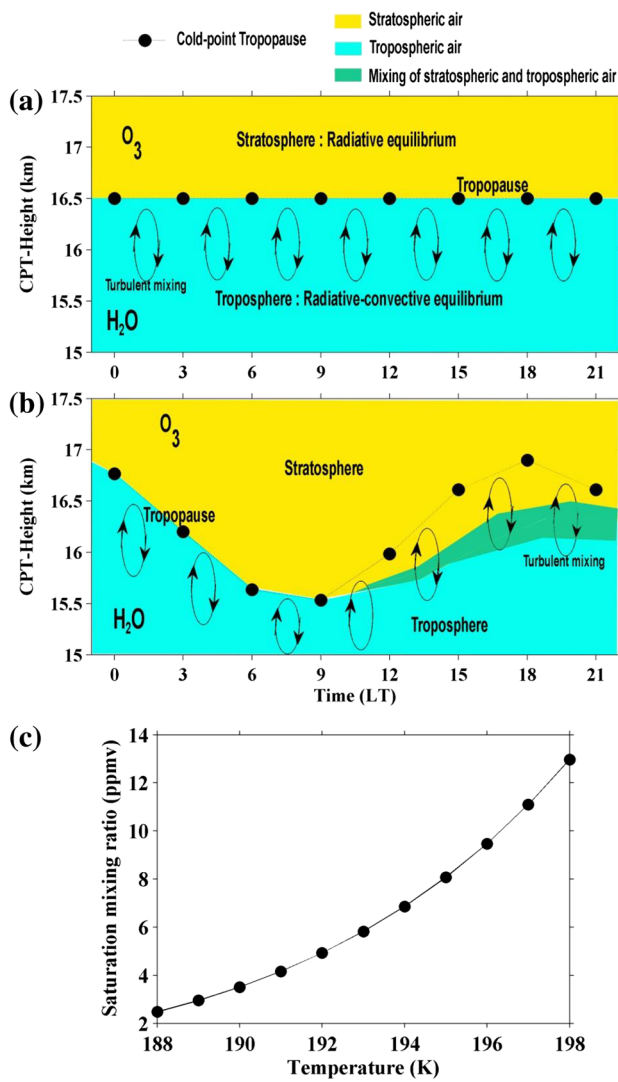


Fig. 8 Thematic figures showing (a) when the tropopause is in steady state, (b) when the tropopause altitude oscillates with time, and (c) relation between the tropopause temperature and saturation mixing ratio

towards the troposphere. The thematic diagram shown in Fig. 8, explains the role of tropopause in exchange and mixing of the air masses between the stratosphere and the troposphere. In Fig. 8, dots indicate the CPT-A. The yellow and blue shaded areas indicate the stratospheric and tropospheric air, respectively. Green shaded area in Fig. 8 b indicates the mixture of the stratosphere- troposphere air. When the tropopause is steady, i.e. no oscillation in the tropopause altitude (Fig. 8a), there will be no exchange of the air masses between the troposphere and the stratosphere. During this stage, the turbulence mixing (occurs within the troposphere) indicated by an ellipse is restricted within the troposphere. When the tropopause altitude oscillates, i.e. descend from ~17 km to 15.5 km (during 0 LT–9

LT), the stratospheric air intrudes downward along with the tropopause as the stratospheric air is highly stable and have a subsidence nature. During the ascending period of the tropopause, i.e. when the tropopause altitude increases from 15.5 to 17 km, during 9–18 LT the stratospheric air, which previously descended along with the tropopause remains at the same lower altitude. Thus, in principle, the stratospheric air is found below the tropopause during 9–18 LT. The turbulence mixing taking place from 0 to 9 LT is well below the tropopause altitude (during the descending phase), whereas from 9 to 18 LT the turbulence mixing attempts to mix the stratospheric air (located below the tropopause) with the tropospheric air. The mixture of stratosphere-troposphere air after 9 LT which is in between the pure stratospheric and tropospheric air is shown as green shade. It illustrates that the stratospheric air partially remains in the troposphere, when the tropopause oscillates from a lower to the higher altitude.

Apart from the tropopause altitude oscillation, the tropopause temperature oscillation plays a significant role in the transport of water vapor from the troposphere to the lower stratosphere (Highwood and Hoskins 1998; Fueglistaler 2009). The holding capacity of the water vapor in the air depends on the saturation mixing ratio according to the Clausius–Clapeyron Equation. The saturation mixing ratio (γ_s) is estimated using the following equation (Bolton 1980 and reference therein)

$$\gamma_s = 0.623 \left(\frac{e_s}{p - e_s} \right) \quad (2)$$

where, the vapor pressure (e_s) is given

$$e_s = 6.11 \times 10^{7.5 \left(\frac{T}{T+237.3} \right)} \quad (3)$$

T is the temperature in °C and p is the pressure in Pa. Figure 8c shows the relation between the tropopause temperature and saturation mixing ratio of water. From the figure, it is clear that the holding capacity of water vapor which depends upon the saturation mixing ratio increases with air temperature. The transport of water vapor from the upper troposphere to the lower stratosphere increases with the tropopause temperature (e.g. Uma et al. 2014). Thus, (a) the tropical CPT-A controls the transport of ozone from the stratosphere to the troposphere, and (b) the tropical CPT-T controls the transport of water vapor through the tropopause.

To support the above hypothesis, we present the day and night difference of ozone and water vapor mixing ratio in the UTLS region, measured using the Aura-MLS. Figure 9 shows the day and night difference of ozone mixing ratio (OMR) at 121, 100, and 82 hPa for two distinguished seasons (DJF and JJA) averaged over the tropical NH (0°–10°N) and the tropical SH (0°–10°S). The 100 hPa

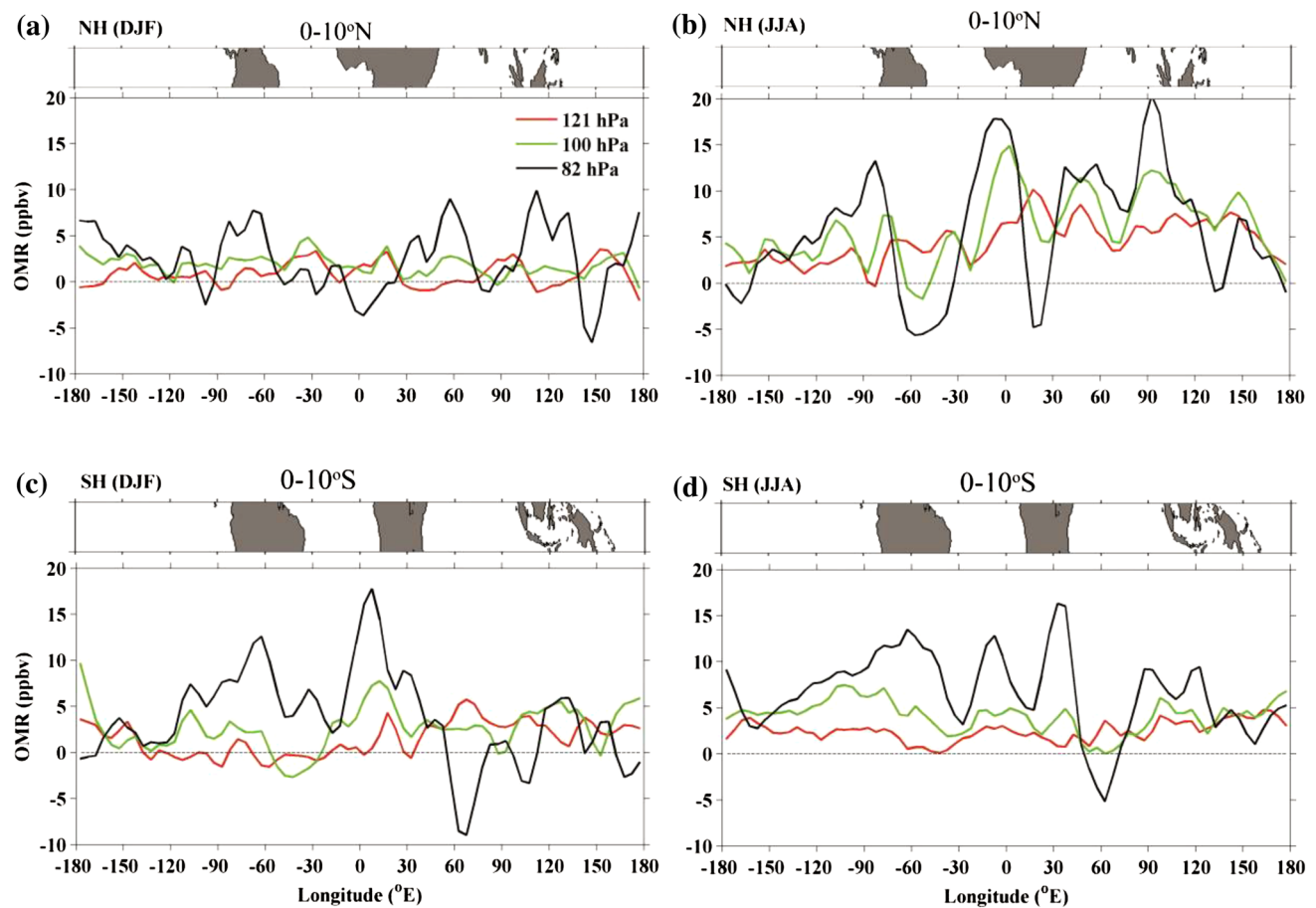


Fig. 9 Longitude variation of day versus night differences of ozone mixing ratio (OMR) at 121, 100 and 82 hPa for (a) NH-DJF, (b) NH-JJA, (c) SH-DJF, and (d) SH-JJA. 7 years (2007–2013) of data are

averaged from 0 to 10°N for NH and 0–10°S for SH. Shaded area in each panel (*top*) indicates the land portion

level roughly corresponds to the tropopause height and 121 hPa and 82 hPa levels are below and above it, respectively. The OMR is higher in the UTLS region during the day, maximizing over the Central Africa, Amazon, Maritime continent and west Pacific in the NH summer. During the SH summer, only the Amazon and Central Africa shows day time ozone maximum. Similar features are also observed in the tropical NH winter and SH winter but the magnitude is smaller than the summer. It is observed that the CPT-A is lowest in the morning and thus we observed maximum ozone during day as that of night. However, it is also to be noted that the OMR difference between the day and night is near to the accuracy of the MLS measurements, thus we cannot discuss the magnitude precisely.

Like the OMR, we also present the day and night difference of the water vapor mixing ratio (WMR) in the UTLS region for both the hemispheres separately and it is shown in Fig. 10. In the tropical NH summer, for 121 hPa (below the tropopause), the day time shows higher WMR over the

Amazon than over Central Africa. At the tropopause level and above it, the day-night difference shows a maximum variation of 0.1 ppmv. The tropical SH summer shows significant enhancement in the day time WMR over the Amazon and Central Africa in the UTLS region. Since the warmer tropopause is observed during forenoon in the SH summer over the Amazon and Central Africa (Fig. 5), thus, we observed more WMR over these region in the day time compared to night. This is due to the fact that the warmer tropopause holds more water vapor compared to the colder tropopause. Over the deep convective regions, winter hemispheres show low WMR in day time in the UTLS region as compared to summer hemisphere.

5.4 Diurnal amplitude of the CPT

To get further insight, diurnal amplitudes of the CPT-A and CPT-T are extracted using least-square fitting (LSF) harmonic analysis. This method is based on a least square fit of

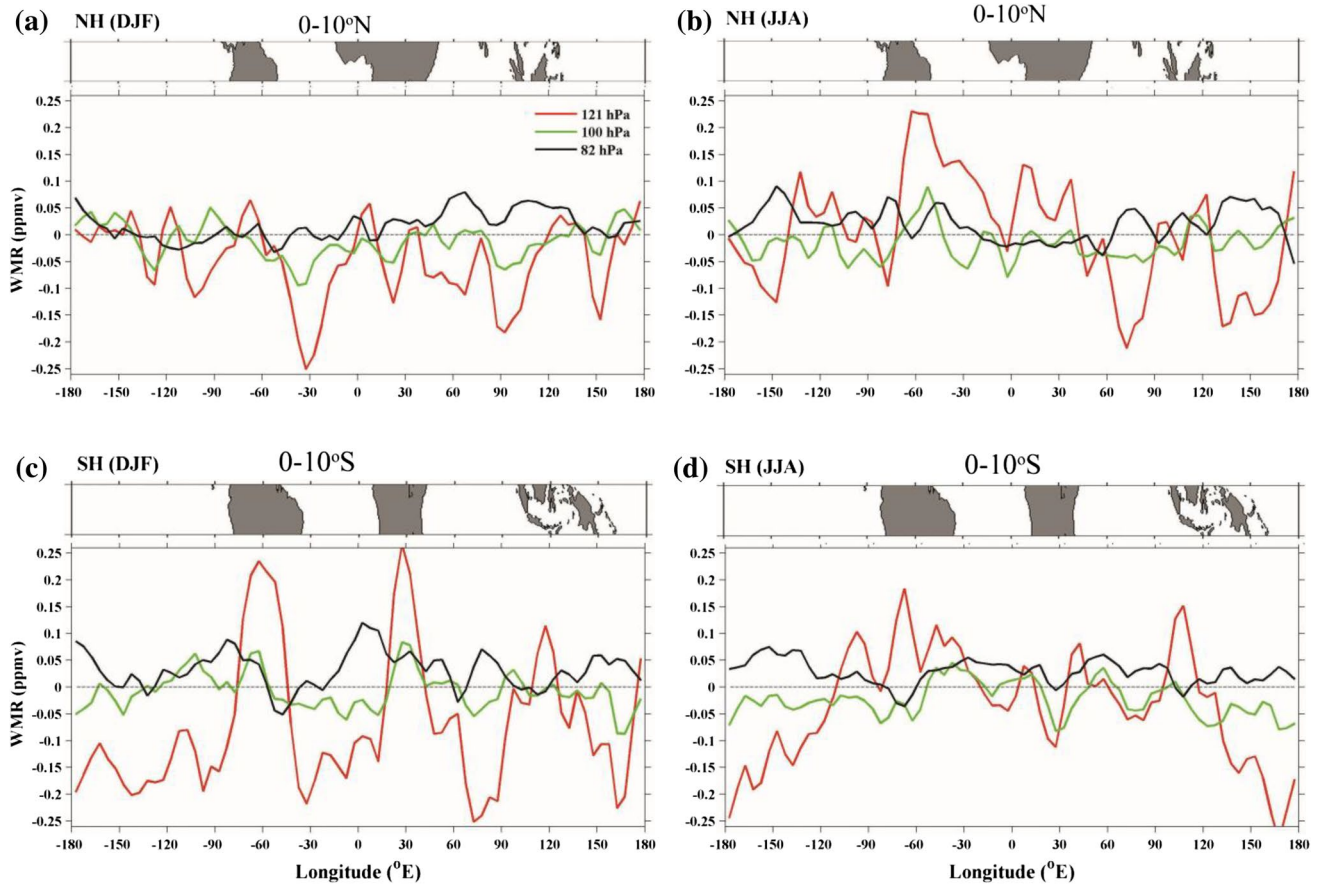


Fig. 10 Same as Fig. 9 but for water vapour mixing ratio (WMR)

sinusoids to data sample with a known frequency (Das et al. 2010 and references therein). In the present analysis, sinusoidal functions with the periods from 1 to 24 h are fitted to the time series of CPT-A and CPT-T. Figure 11 shows the latitude-month distribution of diurnal amplitude of the (a) CPT-A, and (b) CPT-T for land (top) and ocean (bottom). The extracted amplitude is zonally averaged for land and ocean separately. Land shows more diurnal amplitude as compared to the oceans. Maximum diurnal amplitude in the CPT-A and CPT-T is found between 10°S–10°N. In the deep tropical region, the intensity of convection is prevailing over the inter-tropical convergent zone (ITCZ), which is responsible for the enhanced diurnal amplitude in the tropical tropopause. Between 10°S and 10°N, minimum diurnal amplitude in the CPT-T is found during June to September. In Fig. 11, the corresponding averaged phase is shown by the arrows which indicates the time (LT) of occurrence of maximum diurnal variability. With the phase information, it is found that the maximum amplitude in the CPT-A is observed in the late evening during June-July. CPT-T shows the maximum amplitude in the early morning during October to March.

Further analysis is carried out to extract the diurnal amplitude of the zonal mean latitudinal variation of the tropopause. Figure 12 shows the box plot of the zonally averaged latitudinal variation of the diurnal amplitude of the (a) CPT-A, and (b) CPT-T over the land (top) and ocean (bottom) averaged for a period of December 2006 to November 2013. The dots and horizontal bar indicate the mean and median, respectively. The upper and lower whiskers indicate the maximum and minimum values of distributions, and the lower and upper edges of the box indicate the 25 and 75 percentiles, respectively. The highest zonal mean diurnal amplitudes in both the CPT-A and CPT-T are observed in the deep tropics and gradually decrease towards higher latitudes for both land and ocean. The zonal mean diurnal amplitude over the tropical land (ocean) is found to be 130–200 m (140–180 m) for the tropopause altitude and 0.6–0.9 K (0.6–0.8 K) for the tropopause temperature. Further investigations are essential to evaluate the role of atmospheric tides and convection in controlling the diurnal variability of the tropical tropopause.

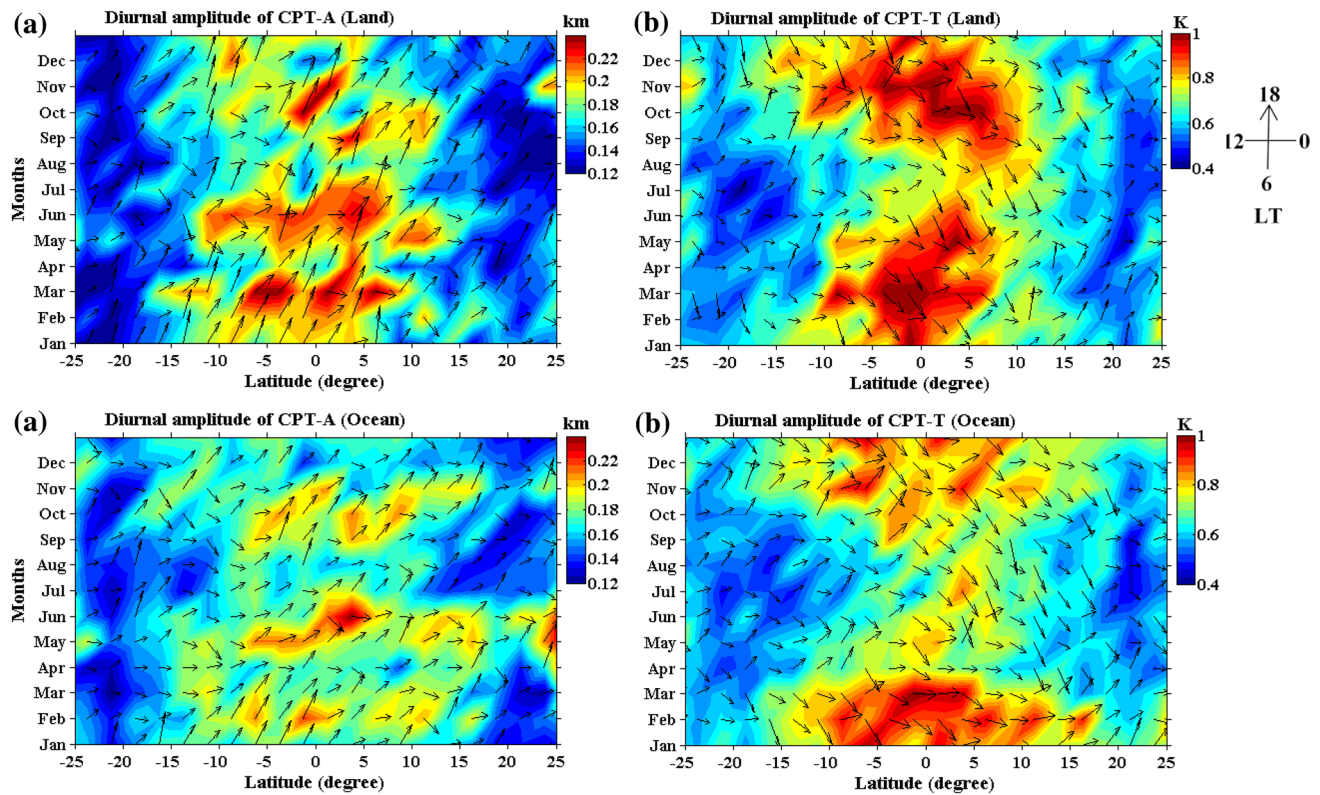


Fig. 11 Zonally averaged latitude-month distribution of the diurnal amplitudes of the CPT (a) altitude, and (b) temperature for land (*top*), and ocean (*bottom*). The data is composite of 7 years from December 2006 to November 2013. The arrows indicate the phase in LT

6 Summary and concluding remark

7 years (December 2006 to November 2013) of the temperature observations made using the COSMIC is utilized to understand the diurnal characteristics of the global tropical tropopause. The Cold-point tropopause altitude and temperature are derived for each temperature profile. Using the equivalent day analysis, a complete diurnal cycle for each month with a time resolution of 3 h is established. The data is further averaged for 2.5° (latitude) $\times 5^\circ$ (longitude). In addition, IR brightness temperature data are used to determine the diurnal variability of deep convection. Influence of diurnal variability of the tropopause on water vapor and ozone in the upper troposphere and lower stratosphere is also studied using Aura-MLS measurements. The following salient features are brought out:

1. The convection is more prominent during afternoon over land and early morning over the Oceans. The land convection is very strong as compared to the oceanic convection.

2. In the deep tropics, higher tropopause altitude over the land (ocean) is observed between evening to late evening (afternoon to early evening).
3. The diurnal variability of the tropopause altitude and temperature is highest over the two deep convective regions, viz. Amazon and Central African in summer hemisphere.
4. More water vapor as well as ozone is found to be higher in the UTLS region during the day as compared to night over the Amazon and Central African regions.
5. The zonal mean diurnal amplitude in the tropopause altitude (temperature) is observed to be 130–200 m (0.6–0.9 K) and 140–180 m (0.6–0.8 K) for land and ocean, respectively.

The present observations of diurnal variability of the global tropical tropopause altitude and temperature reported here is new, and need to be studied further to quantify its role in the exchange of minor constituent between the troposphere and the stratosphere.

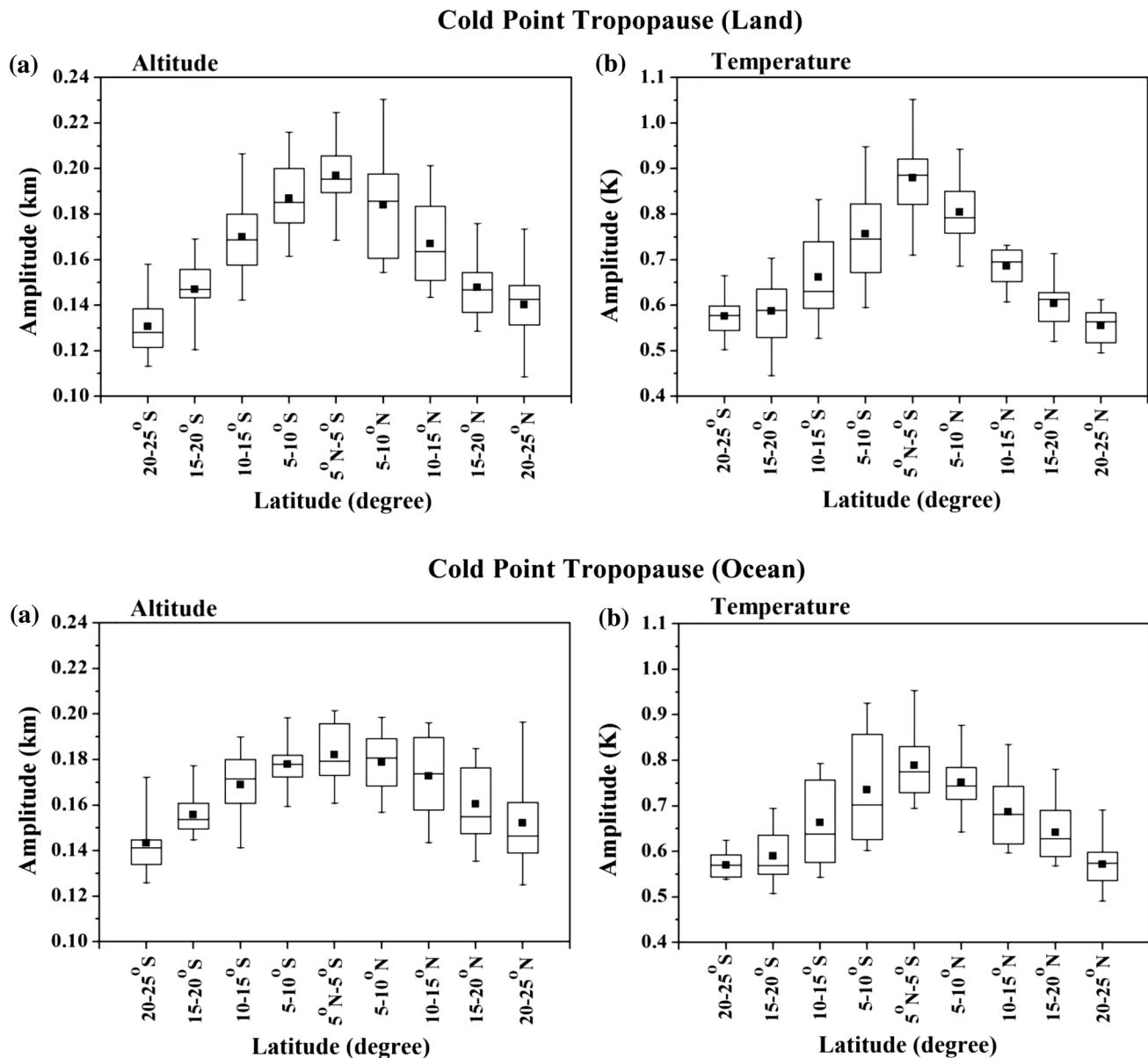


Fig. 12 Latitude variation of the diurnal amplitude of CPT **a** altitude and **b** temperature for land (*top*) and ocean (*bottom*) (see text for details). The amplitude is zonally averaged for a period of December 2006–November 2013

Acknowledgements Authors would like to acknowledge UCAR/CDAAC team for providing the data. Thanks to Director, Space Physics Laboratory (SPL) and Head, Atmospheric Dynamics Branch, SPL for their constant supports extended during this study. The first author KVS thankful to Indian Space Research Organization (ISRO) for providing doctoral fellowship during this study period. Authors would like to sincerely thank both the anonymous reviewers and the editor for their constructive comments and suggestion, which helped the manuscript significantly during the review process.

References

- Alexander P, Torre A, Llamedo P, Hierro R (2014) Precision estimation in temperature and refractivity profiles retrieved by GPS radio occultations. *J Geophys Res* 119:8624–8638
- Biasutti M, Yuter SE, Burleyson CD, Sobel AH (2012) Very high resolution rainfall patterns measured by TRMM precipitation radar: seasonal and diurnal cycles. *Clim Dyn* 39:239–258
- Birner T (2010) Recent widening of the tropical belt from global tropopause statistics: sensitivities. *J Geophys Res* 115:D23109

- Bolton D (1980) The computation of equivalent potential temperature. *Mon Wea Rev* 108:1046–1053
- Chapman S, Lindzen RS (1970) Atmospheric tides thermal and gravitational. D Reidel, Dordrecht, Holland, pp 200
- Das SS, Jain AR, Kumar KK, Narayana Rao D (2008) Diurnal variability of the tropical tropopause: significance of VHF radar measurements. *Radio Sci* 43:RS6003
- Das SS, Kumar KK, Uma KN (2010) MST radar investigation on inertia-gravity waves associated with tropical depression in the upper troposphere and lower stratosphere over Gadanki (13.51°N, 79.21°E). *J Atmos Sol-Terr Phys* 72:1184–1194
- Das SK, Das SS, Chiang CW, Kumar KK, Nee JB (2012) Variability in tropopause height and its temperature on different time scales: An observational study over Banqiao, Taiwan. *J Atmos Sol-Terr Phys* 81:1–8
- Feng S, Fu Y, Xiao Q (2011) Is the tropopause higher over the Tibetan Plateau? Observational evidence from Constellation Observing System for Meteorology, Ionosphere, and Climate (COSMIC) data. *J Geophys Res* 116:D21121
- Forster PM, Shine KP (1999) Stratospheric water vapor changes as a possible contributor to observed stratospheric cooling. *Geophys Res Lett* 26:3309–3312
- Fueglistaler S, Dessler AE, Dunkerton TJ, Folkins I, Fu Q, Mote PW (2009) Tropical tropopause layer. *Rev Geophys* 47:RJ1004
- Fujiwara M, Suzuki J, Gettelman A, Hegglin MI, Akiyoshi H, Shibata K (2012) Wave activity in the tropical tropopause layer in seven reanalysis and four chemistry climate model data sets. *J Geophys Res* 117:D12105
- Gage KS, Reid GC (1985) Response of the tropical tropopause to El Chichon and the El Nino of 1982–1983. *Geophys Res Lett* 12:195–197
- Gettelman A, Salby ML, Sassi F (2002) Distribution and influence of convection in the tropical tropopause region. *J Geophys Res* 107:1–12
- Hajj GA, Ao CO, Iijima BA, Kuang D, Kursinski ER, Mannucci AJ, Meehan TK, Romans LJ, de la Torre Juarez M, Yunck TP (2004) CHAMP and SAC-C atmospheric occultation results and inter-comparisons. *J Geophys Res* 109:06109
- Highwood EJ, Hoskins BJ (1998) The tropical tropopause. *Q J R Meteorol Soc* 124:1579–1604
- Holton JR, Haynes PH, McIntyre ME, Douglass AR, Rood RB, Pfister L (1995) Stratosphere–troposphere exchange. *Rev Geophys* 33:403–439
- Jain AR, Das SS, Mandal TK, Mitra AP (2006) Observations of extremely low tropopause temperature over the Indian tropical region during monsoon and post-monsoon months: possible implications. *J Geophys Res* 111:D07106
- Janowiak JE, Joyce RJ, Yarosh Y (2001) A real-time global half-hourly pixel-resolution infrared dataset and its applications. *Bull Amer Meteor Soc* 82:205–217
- Khaykin SM, Pommereu JP, Hauchecorne A (2013) Impact of land convection on temperature diurnal variation in the tropical lower stratosphere inferred from COSMIC GPS radio occultation. *Atmos Chem Phys* 13:6391–6402
- Kirk-Davidoff DB, Hintsa EJ, Anderson JG, Keith DW (1999) The effect of climate change on ozone depletion through changes in stratospheric water vapor. *Nature* 402:399–401
- Kishore P, Namboothiri SP, Jiang JH, Sivakumar V, Igarashi K (2009) Global temperature estimates in the troposphere and stratosphere: a validation study of COSMIC/FORMOSAT-3 measurements. *Atmos Chem Phys* 9:897–908
- Kuo Y, Wee T, Sokolovskiy S, Rocken C, Schreiner W, Hunt DC, Anthes RA (2004) Inversion and error estimation of GPS Radio Occultation data. *J Meteorol Soc Japan* 82:507–531
- Kursinski ER, Hajj GA, Schofield JT, Linfield RP, Hardy KR (1997) Observing earth's atmosphere with radio occultation measurements using the global positioning system. *J Geophys Res* 102:23429–23465
- Liu Y, Xu T, Liu J (2014) Characteristics of the seasonal variation of the global tropopause revealed by COSMIC/GPS data. *Adv Space Res* 54:2274–2285
- Livesey NJ, Read WG, Froidevaux L, Lambert A, Manney GL, Pumphrey HC et al (2011) EOS MLS version V3.3 level 2 data quality and description document. Jet Propul Lab Pasadena, CA. <http://mls.jpl.nasa.gov>
- Meenu S, Rajeev K, Parameswaran K, Nair AKM (2010) Regional distribution of deep clouds and cloud top altitudes over the Indian subcontinent and the surrounding oceans. *J Geophys Res* 115:D05205
- Pirscher B, Foelsche U, Lackner BC, Kirchengast G (2007) Local time influence in single-satellite radio occultation climatologies from Sun-synchronous and non-Sun-synchronous satellites. *J Geophys Res* 112:D11119
- Rieckh T, Scherllin-Pirscher B, Ladstädter F, Foelsche U (2014) Characteristics of tropopause parameters as observed with GPS radio occultation. *Atmos Meas Tech* 7:3947–3958
- Rind D, Lonergan P (1995) Modeled impacts of stratospheric ozone and water vapor perturbations with implications for high-speed civil transport aircraft. *J Geophys Res* 100:7381–7396
- Scott RK, Cammas JP (2002) Wave breaking and mixing at the subtropical tropopause. *J Atmos Sci* 59:2347–2361
- Seidel DJ, Randel WJ (2006) Variability and trends in the global tropopause estimated from radiosonde data. *J Geophys Res* 111:D21101
- Seidel DJ, Ross RJ, Angell JK, Reid GC (2001) Climatological characteristics of the tropical tropopause as revealed by radiosondes. *J Geophys Res* 106:7857–7878
- Seidel DJ, Fu Q, Randel WJ, Reichler TJ (2008) Widening of the tropical belt in a changing climate. *Nat Geosci* 1:21–24
- Shimizu A, Tsuda T (2000) Variations in tropical tropopause observed with radiosondes in Indonesia. *Geophys Res Lett* 27:2541–2544
- Smith EK, Weintraub S (1953) The constants in the equation for atmospheric refractive index at radio frequencies. *J Res Natl Bur Stand* 50:39–41
- Thuburn J, Craig GC (2002) On the temperature structure of the tropical substratosphere. *J Geophys Res* 107:D2
- Tian B, Soden BJ, Wu X (2004) Diurnal cycle of convection, clouds, and water vapor in the tropical upper troposphere: Satellite versus a general circulation model. *J Geophys Res* 109:D10101
- Tsuda T, Murayama Y, Wiryo Sumarto H, Harijono SWB, Kato S (1994) Radiosonde observations of equatorial atmosphere dynamics over Indonesia: 1. Equatorial waves and diurnal tides. *J Geophys Res* 99:10491–10505
- Tsuda T, Lin X, Hayashi H, Noersomadi (2011) Analysis of vertical wave number spectrum of atmospheric gravity waves in the stratosphere using COSMIC GPS radio occultation data. *Atmos Meas Tech* 4:1627–1636
- Uma KN, Das SS (2016) Quantitative and qualitative assessment of diurnal variability in tropospheric humidity using SAPHIR onboard Megha-Tropiques. *J Atmos Sol-Terr Phys* 146:89–100
- Uma KN, Das SK, Das SS, Kumar KK (2013a) Aura-MLS observations of water vapor entering the stratosphere over the Northern bay of Bengal and East Equatorial Indian Ocean. *Terr Atmos Ocean Sci* 24:357–368
- Uma KN, Kumar KK, Das SS (2013b) Migrating and non-migrating diurnal and semi-diurnal tides over a tropical and an equatorial station. *Indian J Radio and Space Phys* 42:340–355
- Uma KN, Das SK, Das SS (2014) A climatological perspective of water vapor at the UTLS region over different global monsoon regions: observations inferred from the Aura-MLS and reanalysis data. *Clim Dyn* 43:407–420

- World Meteorological Organization (WMO) (1957) Meteorology-a three-dimensional science: second session of the commission for aerology. WMO Bull IV(4):134–138
- Xian T, Fu, Y (2015) Characteristics of tropopause-penetrating convection determined by TRMM and COSMIC GPS radio occultation measurements. *J Geophys Res* 120:7006–7024
- Xie F, Wu DL, Ao CO, Mannucci AJ (2010) Atmospheric diurnal variations observed with GPS radio occultation soundings. *Atmos Chem Phys* 10:6889–6899
- Yamamoto Masayuki K, Oyamatsu Masayuki, Horinouchi Takeshi, Hashiguchi Hiroyuki, Fukao Shoichiro (2003) High time resolution determination of the tropical tropopause by the equatorial atmosphere radar. *Geophys Res Lett* 30:2094
- Zhang X, Forbes JM, Hagan ME, Russell JM III, Palo SE, Mlynczak M (2006) Monthly tidal temperatures 20–120 km from TIMED/SABER. *J Geophys Res* 111:A10208